END
DATE
FILMED

4 -84

DTIC

MICROCOPY RESOLUTION TEST CHART

NATIONAL BUREAU OF STANDARDS-1963-A

AFWAL-TR-83-2094

PROOF OF PRINCIPLE EXPERIMENT FOR A COHERENT CO_2 WAVEGUIDE LASER ARRAY

Douglas G. Youmans
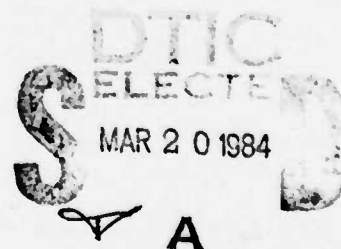W. J. Schafer Associates, Inc.
Corporate Place 128, Building 2, Suite 300
Wakefield, MA 01880

January 1984

Final Report for Period July 1982 - October 1983

Approved for public release; distribution unlimited.

AD A139121

AERO PROPULSION LABORATORY
AIR FORCE WRIGHT AERONAUTICAL LABORATORIES
AIR FORCE SYSTEMS COMMAND
WRIGHT PATTERSON AIR FORCE BASE, OHIO 45433

DTIC
ELECTE
MAR 2 0 1984

A

84 03 19 004

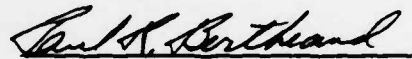PETER BLETZINGER, Proj Engr
Energy Conversion Branch

PAUL R. BERTHEAUD
Chief, Energy Conversion Branch
Aerospace Power Division
Aero Propulsion Laboratory

FOR THE COMMANDER

JAMES D. REAMS
Chief, Aerospace Power Division
Aero Propulsion Laboratory

REPORT DOCUMENTATION PAGE

1a. REPORT SECURITY CLASSIFICATION UNCLASSIFIED		1b. RESTRICTIVE MARKINGS			
2a. SECURITY CLASSIFICATION AUTHORITY		3. DISTRIBUTION/AVAILABILITY OF REPORT Approved for public release; distribution unlimited.			
2b. DECLASSIFICATION/DOWNGRADING SCHEDULE					
4. PERFORMING ORGANIZATION REPORT NUMBER(S) WJSA-FR-83-241		5. MONITORING ORGANIZATION REPORT NUMBER(S) AFWAL-TR-83-2094			
6a. NAME OF PERFORMING ORGANIZATION W.J. Schafer Associates, Inc.	6b. OFFICE SYMBOL (If applicable)	7a. NAME OF MONITORING ORGANIZATION AFWAL/POOC-3			
6c. ADDRESS (City, State and ZIP Code) Corporate Place 128, Bldg. 2, Suite 300 Wakefield MA 01880		7b. ADDRESS (City, State and ZIP Code) Wright-Patterson AFB, OH 45433			
8a. NAME OF FUNDING/SPONSORING ORGANIZATION	8b. OFFICE SYMBOL (If applicable)	9. PROCUREMENT INSTRUMENT IDENTIFICATION NUMBER F33615-82-C-2217			
8c. ADDRESS (City, State and ZIP Code)		10. SOURCE OF FUNDING NOS.			
		PROGRAM ELEMENT NO. 61102F	PROJECT NO. 2301	TASK NO S2	WORK UNIT NO. 95

11. TITLE (Include Security Classification)
Proof of Principle Experiment for A Coherent CO_2 Waveguide Laser Array

12. PERSONAL AUTHOR(S)
D. G. Youmans, E. Locke, E. Hoag, G. Zeiders

13a. TYPE OF REPORT Final	13b. TIME COVERED FROM 820701 TO 83103	14. DATE OF REPORT (Yr., Mo., Day) 8401	15. PAGE COUNT 34

16. SUPPLEMENTARY NOTATION

17.	COSATI CODES		18. SUBJECT TERMS (Continue on reverse if necessary and identify by block number)
FIELD	GROUP	SUB. GR.	Laser Waveguide CO_2, Leaky Mode Coupling, Laser, CO_2,
20	5	1	Waveguide Laser Zinc Selenide (ZnSe)

Carbon dioxide

19. ABSTRACT (Continue on reverse if necessary and identify by block number)

A method is investigated to increase the output of small waveguide lasers by coupling several waveguides using leaky modes through the waveguide walls. The theoretical part of the work establishes the advantages of the coupled mode operation versus output from a corresponding array of uncoupled waveguide lasers as the increase of the "power in the bucket" in the far field. The problems of optimum gas mixtures and questions of thermal management are treated also. An experimental test of suitable waveguide materials showed that relatively rough surfaced and therefore less expensive ZnSe material has sufficiently low losses. Initial experiments using RF excitation into the waveguides or one single waveguide were unsuccessful due to difficulties in matching RF generator and load. Operation with DC resulted in output powers meeting specifications. A test of two parallel waveguides separated by a ZnSe wall showed coupling of the two lasing channels, if they operated on the same laser transition. This was tested with a pyroelectric detector array which showed the coherent summation of the two far field patterns.

20. DISTRIBUTION/AVAILABILITY OF ABSTRACT UNCLASSIFIED/UNLIMITED ☒ SAME AS RPT. ☐ DTIC USERS ☐	21. ABSTRACT SECURITY CLASSIFICATION UNCLASSIFIED	
22a. NAME OF RESPONSIBLE INDIVIDUAL P. Bletzinger	22b. TELEPHONE NUMBER (Include Area Code) 513-255-2923	22c. OFFICE SYMBOL AFWAL/POOC-3

DD FORM 1473, 83 APR   EDITION OF 1 JAN 73 IS OBSOLETE.

TABLE OF CONTENTS

LIST OF FIGURES

LIST OF TABLES

PROOF OF PRINCIPLE EXPERIMENT FOR A COHERENT CO_2 WAVEGUIDE LASER ARRAY

1.0 CO_2 WAVEGUIDE LASER ARRAY CONCEPT

Waveguide CO_2 lasers are a technologically well developed and widely used source of coherent laser radiation. Applications have included laser designators, master oscillators, local oscillators, coherent laser radars, tunable IR spectroscopy, low power cutting and heating of materials, as well as general laboratory usage. A typical waveguide CO_2 laser consists of a bore or groove one or two millimeters in cross-section in a ceramic or similar material. An electrical discharge is run down or across the bore to excite the gain medium. The bore confines or "guides" the IR radiation, thus the recirculating radiation does not obey the laws of free space propagation as in conventional lasers. Because the bore confines both the gain medium and the laser radiation to the same region, very compact and reasonably efficient devices are possible. A typical waveguide CO_2 laser might be packaged into a 2" x 2" x 12" box having an output power of 30W multi-line.

In an effort to obtain higher output powers from nearly the same size package, Dr. Howard Schlossberg of the Air Force Office of Scientific Research suggested forming an n x m array of such waveguide lasers. Such a device is conceptually illustrated in Fig. 1.1. Each waveguide laser would leak radiation into the adjacent laser causing them to "lock" together at the same frequency and the same phase. Such an array of phase-locked waveguide laser would have (n x m) times as much near-field power but also an $(n \times m)^2$ increase in the peak of the far-field laser irradiance distribution. (The total power will of course remain (n x m) times as large as that of a single laser.) This is analogous to a multiple slit interference pattern illustrated in Fig. 1.2.

-1-
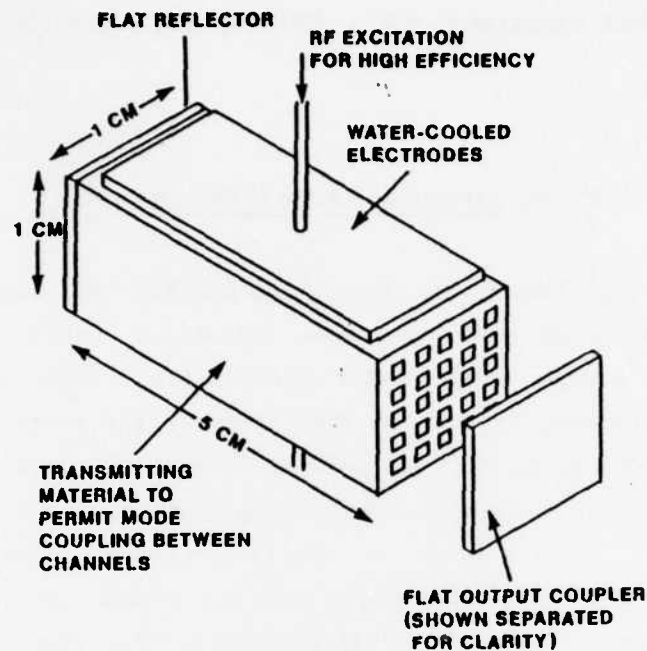
Figure 1.1. CO$_2$ Waveguide Laser Array

NOTE THAT PHASE-LOCKING
CONCENTRATES ENERGY IN
WIDELY-SPACED ORDERS —
AN UNDESIRABLE RESULT
FOR MANY APPLICATIONS
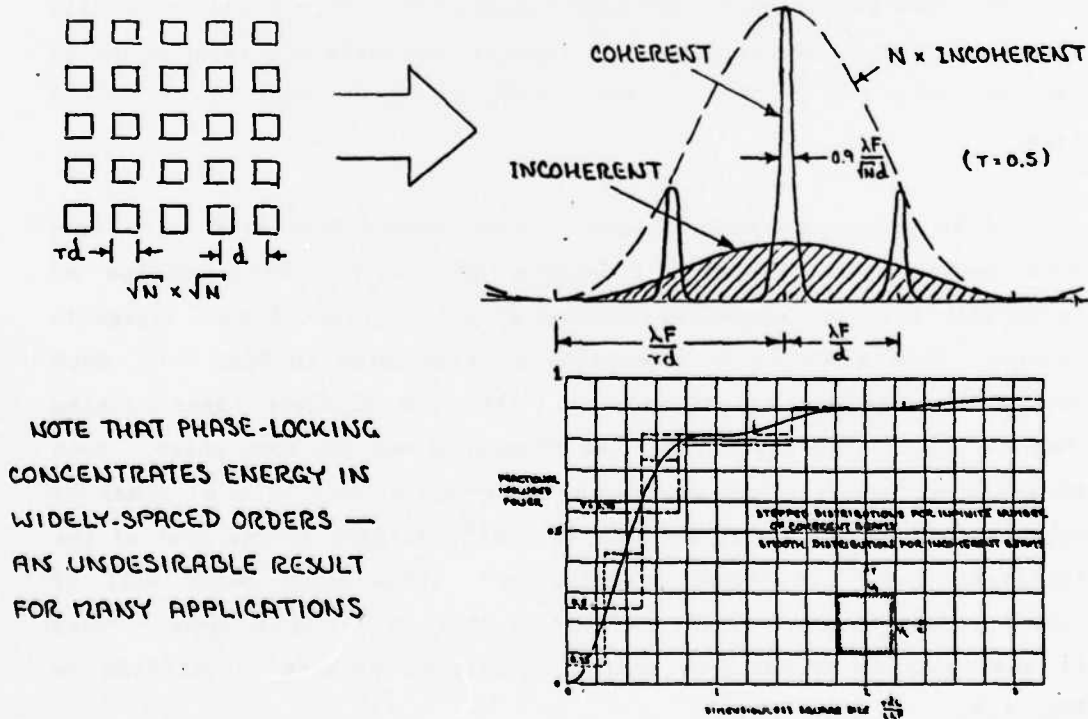
Figure 1.2. Multiple Slit Interference Pattern

The purpose of this contract was to verify that it is possible to phase-lock adjacent waveguide lasers by leaking a small amount of laser radiation between the waveguides. The successful demonstration of phase-locking is presented in section 6.0. Other experimental results are given in sections 4.0 and 5.0. Analyses of waveguide CO_2 lasers are presented in sections 2.0 and 3.0, and future work is suggested in section 7.0. Note that although the CO_2 lasing medium is considered and experimentally tested in this report, the concept is not limited to CO_2 laser devices.

2.0 REVIEW OF WAVEGUIDE LASER THEORY

In order to fabricate an array of waveguide CO_2 lasers, it is necessary to review the basic theory and experimental data given in the electro-optical literature. This forms the starting point for designing and analyzing the test devices. It also forms a convenient reference section for the effects of waveguide laser and associated component modifications as they arise.

The analysis of the properties of waveguide lasers consists of determining the waveguiding losses due to the propagation of the electromagnetic field inside the waveguide and the losses of coupling this field into and out of the waveguide when reflecting off of the cavity mirrors. Next, for a given set of small signal gains and saturation parameters, laser output powers can be calculated using a Rigrod analysis for homogeneous lasers. The small signal gains and saturation parameters of the CO_2 laser media as a function of pressure, temperature, and discharge current are discussed in the subsequent section.

2.1 Waveguide Modes and Loss Coefficients

CO_2 waveguide lasers are constructed of hollow dielectric waveguides as opposed to common solid fiber-optic waveguides. The electromagnetic wave boundary conditions are at the sides of the cavity as well as at the ends as in a conventional laser cavity.

2.1.1 Circular Hollow Dielectric Waveguides. Marcatili and Schmeltzer[1] were among the first to analyze hollow delectric waveguides. They showed that the electric and magnetic fields were functions of Bessel functions and the modes could be circular electric, circular magnetic, or hybrid with all components present. In general, the lowest-loss mode is the hybrid mode EH_{11}. The EH_{nm} loss coefficient is given by

-4-

$$\alpha_{nm} = \left(\frac{u_{nm}}{2\pi}\right)^2 \frac{8\lambda^2}{a^3} \, \mathrm{Re} \, \left\{\frac{1/2\left(n^2 + 1\right)}{\left(n^2 - 1\right)^{1/2}}\right\} \tag{1}$$

where

a = waveguide radius

u_{nm} = m^{th} root of J_{n-1}

u_{11} = 2.405

$n = n' - ik$ complex refractive index of waveguide material

The loss coefficient is seen to be proportional to λ^2 and inversely proportional to a^3. The bore radius cannot be made arbitrarily large, however, as this would allow higher order transverse mode operation and not confine and control the discharge.

The loss coefficients of the EH_{11} mode for various materials are

$$\alpha_{11} = 4.3 \times 10^{-5} \text{cm}^{-1} \text{ for BeO (ref. 2)}$$
$$= 1.8 \times 10^{-3} \text{cm}^{-1} \text{ for SiO}_2 \text{ (ref. 2)}$$
$$= 1.6 \times 10^{-2} \text{cm}^{-1} \text{ for ZnSe}$$

for a = 0.5mm radius at λ = 10.6µm.

Also, Abrams[3] showed that the Gaussian TEM_{00} mode which most closely matches the EH_{11} mode is that with a $1/e^2$ intensity beam radius of

$$w_o = 0.6435a \tag{2}$$

The $1/e^2$ divergence out of the waveguide is therefore

$$\theta = \frac{2}{\pi} \frac{\lambda}{\omega_o} \text{ (full angle)}$$

$$\cong \frac{2}{\pi} \frac{\lambda}{0.6435a} \tag{3}$$

$$= 21 \text{mr (radius = 0.5mm)}$$

-5-

2.1.2 <u>Rectangular Hollow Dielectric Waveguides</u>. The rectangular case was analyzed by Krammer[4] and Laakman and Steier[5]. Only hybrid modes, EH_{nm}, are supported having the form

$$H_x = -E_y \sqrt{\frac{\varepsilon_o}{\mu_o}} = M \left\{ \begin{matrix} \cos(p_1 \pi x/2a) \\ \sin(p_2 \pi x/2a) \end{matrix} \right\} \left\{ \begin{matrix} \cos(q_1 \pi y/2b) \\ \sin(q_2 \pi y/2b) \end{matrix} \right\}$$

$$H_z = \pi M/2jka \left\{ \begin{matrix} -p_1 \sin(p_1 \pi x/2a) \\ p_2 \cos(p_2 \pi x/2a) \end{matrix} \right\} \left\{ \begin{matrix} \cos(q_1 \pi y/2b) \\ \sin(q_2 \pi y/2b) \end{matrix} \right\} \qquad (4)$$

$$E_z = -\pi M \sqrt{\frac{\mu_o}{\varepsilon_o}} /2jkb \left\{ \begin{matrix} \cos(p_1 \pi x/2a) \\ \sin(p_2 \pi x/2a) \end{matrix} \right\} \left\{ \begin{matrix} -q_1 \sin(q_1 \pi y/2b) \\ q_2 \cos(q_2 \pi y/2b) \end{matrix} \right\}$$

$$p_1, \ q_1 \text{ odd}$$
$$\text{or}$$
$$p_2, \ q_2 \text{ even}$$

for the EH_{nm}^x modes with similar equations for the EH_{nm}^y modes. The waveguide is 2a x 2b in dimension, M is a constant, and the mode propagates in the z direction.

The attenuation coefficient is

$$\alpha_{pq} = \frac{(p\pi)^2}{4k^2 a^3} \ \text{Re}\left\{ \frac{1}{\sqrt{n^2 - 1}} \right\} + \frac{(q\pi)^2}{4k^2 b^3} \ \text{Re}\left\{ \frac{n^2}{\sqrt{n^2 - 1}} \right\} \qquad (5)$$

and for the EH_{11} mode with a = b

$$\alpha_{11} = \frac{\lambda^2}{16a^3} \ \text{Re}\left\{ \frac{n^2 + 1}{\sqrt{n^2 - 1}} \right\}$$

$$= 1.74 \times 10^{-3} \text{cm}^{-1} \text{ for ZnSe } (a = 0.5\text{mm})$$
$$= 1.6 \times 10^{-4} \text{cm}^{-1} \text{ for SiO}_2 \ (a \equiv 0.5\text{mm}) \text{ (ref. 5)}$$
$$= 3.0 \times 10^{-5} \text{cm}^{-1} \text{ for BeO } (a \equiv 0.5\text{mm}) \text{ (ref. 5)}$$
$$= 1.8 \times 10^{-4} \text{cm}^{-1} \text{ for Al}_2\text{O}_3 \ (a \equiv 0.5\text{mm}) \text{ (ref. 5)}$$

Also Laakman and Steier[5] and Henderson[6] showed that the matching TEM_{00} beam waist is

$$\omega_o = 0.69a \qquad (6)$$

Thus, the $1/e^2$ intensity full angle divergence is

$$\theta = \frac{2\lambda}{\pi\omega_o} = \frac{2\lambda}{\pi(0.69)a} = 19.6mr \qquad (7)$$

from a 2a x 2a of 1m x 1mm waveguide.

2.2 Input/Output Coupling Losses

Degnan and Hall[6] showed that there are three mirror (or lens) locations for maximum mode coupling (minimum loss) of the reflected radiation back into the waveguide:

1. A flat mirror at the end of the waveguide
2. A distant mirror with radius of curvature equal to the distance from the waveguide aperture
3. A mirror at the Rayleigh range, $\dfrac{\pi\omega_o^2}{\lambda}$, with a curvature of twice this distance

For the waveguides of interest in this experiment, case 1 is the important condition. Degnan and Hall[6] showed that as the flat mirror is slightly moved away from the waveguide aperture, the coupling losses are approximately given by

$$loss \cong 6.05 \left(\frac{2\pi z}{\lambda a^2}\right)^{3/2}$$

$$= 1.7\% \text{ at } z = 3mm$$
$$= 2.7\% \text{ at } z = 4mm$$
$$= 3.8\% \text{ at } z = 5mm$$

$$(8)$$

where z is the aperture to mirror distance.

2.3 Rigrod Output Power Analysis

We are now able to perform a first order analysis of the waveguide laser output power for varius small signal gains and output couplings. Rigrod[8] and Casperson[9] have shown that the output power from a homogeneously broadened laser is approximately given by

$$P_{out} = \frac{I_s}{2} At \left[\frac{2g_o l}{t + L} - 1\right] \qquad (9)$$

where

$$I_s = \left\{ \begin{array}{l} 4,000W/cm^2 \text{ (100 torr) (ref. 2)} \\ 15,000W/cm^2 \text{ (200 torr) (ref. 2)} \end{array} \right. \text{ saturation intensity}$$

$A = 1mm \times 1mm$ area $\times \pi/4$ (~ mode area)

$t =$ transmission of output coupler

$g_o =$ small signal gain

$l =$ discharge length $= 9.4cm$

$L =$ losses other than output transmission
$\cong 2 \times 4\%$ (waveguide loss) $+ 1\%$ (reflector) $+ 2 \times (1.7\%)$ (coupling)
$\cong 12.4\%$

Substituting for various small signal gains, g_o, and output coupler transmissions, t, the following tables can be formed:

TABLE I. OUTPUT POWER/CHANNEL AT 100 TORR (W)

$g_o(cm^{-1})$	0.97	0.96	0.93	0.90	0.87	0.84	OUTPUT COUPLER REFLECTIVITY
0.01	0.10	0.09	0	0	0	0	
0.015	0.39	0.45	0.50	0.40	0.23	0	
0.02	0.68	0.81	1.03	1.06	0.98	0.81	
0.03	1.25	1.50	2.10	2.38	2.49	2.48	

TABLE II. OUTPUT POWER/CHANNEL AT 200 TORR (W)

$g_0(cm^{-1})$	0.97	0.96	0.93	0.90	0.87	0.84	OUTPUT COUPLER REFLECTIVITY
0.01	0.37	0.34	0	0	0	0	
0.015	1.46	1.69	1.88	1.50	0.86	0	
0.02	2.55	3.04	3.86	3.98	3.68	3.04	
0.03	4.67	5.62	7.87	8.92	9.34	9.30	

The solid line indicates optimum output coupling and maximum laser power. Note that the optimum output coupling determined by differentiating eq. (9) is given by

$$t_{opt} = (2g_0 1L)^{1/2} - L \qquad (10)$$

once g_0 and round trip loss, L, are known.

From Tables I and II it can be seen that in the region of small signal gains of 1% to 2% per cm, output couplings of 3% to 7% or reflectivities of 97% to 93% are optimum. The saturation parameters, I_s, are taken from ref. 2, and in actuality the small signal gain at 200 torr would be less than that at 100 torr. The waveguide loss of 4% is taken from section 4.0. This overview allows us to see what the expected output powers will be for different output couplings within the small signal gain values of the CO_2 medium.

3.0 <u>ANALYSIS OF CO_2 LASER GAIN MEDIA PROPERTIES</u>

An extensive computer analysis of waveguide CO_2 laser small signal gain, gas temperature, and tunability as functions of total pressure, $He:N_2:CO_2$ ratios, tube diameter, and electron excitation rate of N_2 was published by S. Cohen in ref. 10. Some of the important results of this study are as folows:

1. The P(20) transition peak small signal gain varies from about 1.0% to 2.0% for most gas mixtures over a total pressure range of from 60 torr to 150 torr.

2. At 50 torr pressure maximum gain occurs at a 2:1:1 or 2:0.5:1 = $He:N_2:CO_2$ ratio, while at 150 torr the gain maximum shifts to the 5 to 7:1:1 region. This is in good agreement with the experimental data of section 6.0.

3. Small signal gain decreases almost linearly with increasing wall temperature, and for each pressure there is an optimal bore diameter which maximizes gain -- typically from 0.5 to 1.5mm diameter.

4. Transition frequency width (tunabilty) peaks at some optimal pressure which is a function of cavity optical loss and length.

Reference 10 does not calculate expected laser output powers as a function of gas parameters nor does he compute saturation intensities needed for a first order Rigrod analysis of section 2.3. Since the saturation intensity is approximately proportional to (pressure)^2, maximum laser outputs occur at a pressure higher than the maximum small signal gain pressure as shown in ref. 2.

Glenn Zeiders also performed an output power analysis of a bulk CO_2 laser medium using the gas parameters given in the Avco Everett Research Laboratory Laser Kinetics Handbook[15]. Power density into the upper and lower lasing vibration levels is given by

$$\left(R_3 + \frac{\theta_3}{\theta_\nu} R_N\right) \frac{jE}{p^2 \psi_{CO_2}} = \frac{\theta_3/T}{p\tau_3} \frac{r - \bar{r}(s/\bar{s})^3}{(1 - r)(1 - s)^3} + \frac{\theta_3}{\theta_\nu} \frac{gI}{p^2 \psi_{CO_2}} \quad (11)$$

$$R_2 \frac{jE}{p^2 \psi_{CO_2}} + \frac{3\theta_2/T}{p\tau_3} \frac{r - \bar{r}(s/\bar{s})^3}{(1 - r)(1 - s)^3} + \left(\frac{\theta_3}{\theta_\nu} - 1\right) \frac{gI}{p^2 \psi_{CO_2}} = \frac{2\theta_2/T}{p\tau_2} \frac{s - \bar{s}}{1 - s} \quad (12)$$

Optical gain is given by

$$g = \frac{\Gamma_1 \Gamma_2}{\Gamma_3} \psi_{CO_2} \frac{512}{T} (1 - r)(1 - s)^2 (1 - s^2) [r - s^{2.08} e^{-1.13 \frac{J + 1}{T}}] \quad (13)$$

Gas heating is

$$0 = jE - gI = \frac{16k}{D^2} (T_C - T_{wall}) \quad (14)$$

The parameters are

R_i = pumping efficiency of ith vibrational level

θ_i = vibrational energy of ith state

j = discharge current density A/cm^2

E = discharge volts/cm

p = gas pressure

ψ_{CO_2} = molar fraction of CO_2

τ_i = energy transfer time of ith level

T = gas temperature (T_C at center, T_{wall} at wall)

-11-

r = CO_2 fraction in upper lasing state wrt ground state

s = CO_2 fraction in lower lasing state wrt ground state

$\bar{r}$,$\bar{s}$ = ambient temperature Boltzman distributions

$\Gamma_1, \Gamma_2, \Gamma_3$ = rotational gain, doppler factor, and mixture dependent parameters of order unity

D = bore diameter

k = thermal diffusion coefficent

In Figs. 3.1 and 3.2 are plotted input power versus output power as a function of g/ψ_{CO_2} for a He:CO_2 mixture and a 6:4:1 = He:N_2:CO_2 mixture, respectively. From these complicated plots it can be shown that maximum ouput occurs at a power loading of $RjE/p^2\psi_{CO_2} \cong 80W/mm^3/atm^2$. Choosing a thermal diffusion coefficeint of $k = 7 \times 10^{-4}W/cm^\circ$ C and a gas ΔT of 150°, $Q^2D = 1.7W/cm$, and therefore conductive heat dissipation limits power input/length to $jED^2 = 1.7W/cm$. Substituting back into eqs. (11) and (12), the optimum $pD\sqrt{\psi_{CO_2}}$ product equals about 0.04 atm-mm.

Inputting 210W into twenty-five 5cm cavities produces greater than 20W of output power assuming a 10% optical cavity loss and 100 torr pressure with ψ_{CO_2} = 0.1. The plots indicate that these conditions are near optimum, but the pressure can be raised to 200 torr without severe loss. These operating conditions and power loadings are in reasonable agreement with the measured data of section 6.2.
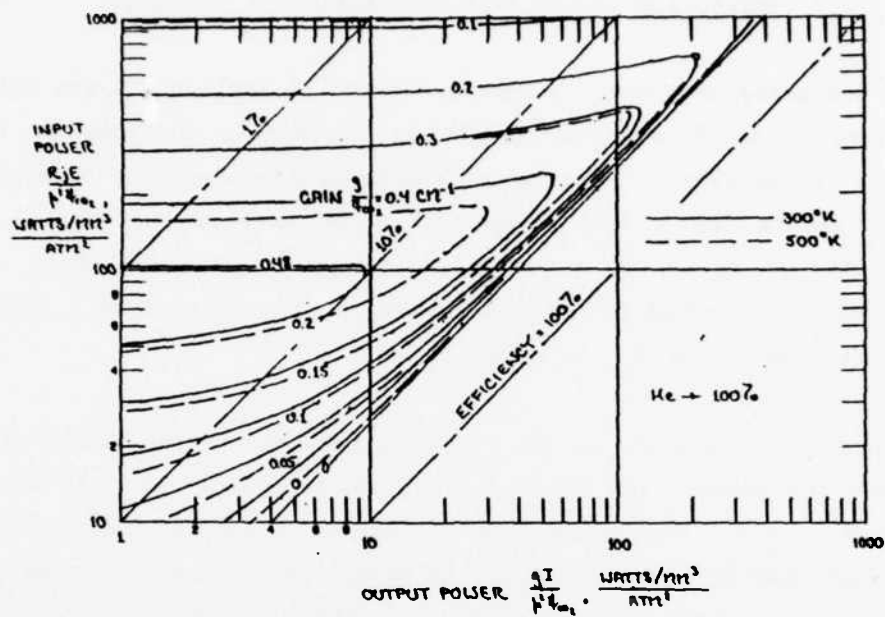
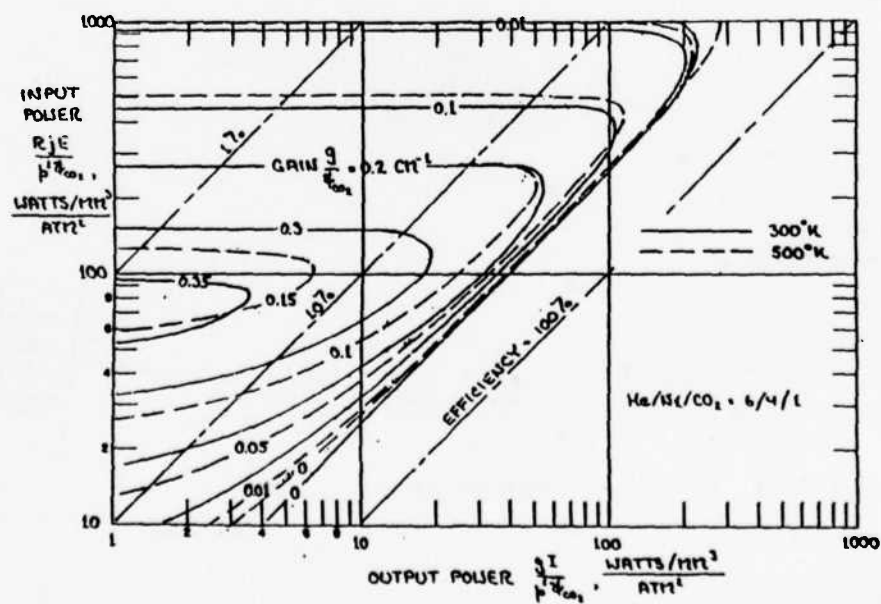Figure 3.1.   Steady State Power Extraction, He:CO_2

Figure 3.2.   Steady State Power Extraction, 6:4:1

4.0   REFLECTION LOSSES FROM ZnSe WAVEGUIDE SURFACES

The waveguide loss coefficients presented in section 2.1 are valid for optically smooth and optically flat dielectric surfaces on the insides of the waveguide. Because of the prohibitive cost of obtaining optically smooth 1mm x 1mm grooves in ZnSe as shown in Fig. 1.1, grinding the grooves using a one millimeter thick grinding wheel was the only feasible method of obtaining waveguides. Grooves were ground in both the ZnSe and Al_2O_3 dielectric materials.

In order to determine if the rough surface scattering losses were too severe for waveguiding applications, an experiment was set up as shown in Fig. 4.1.   The reflection at 10.6µm off of frosted, ground, and polished ZnSe at large angles of incidence can be measured relative to the aluminum coated reference mirror.   The frosted surface is the coarsest surface, the ground surface corresponds to that of the waveguide surfaces, and the polished surface is optically smooth.
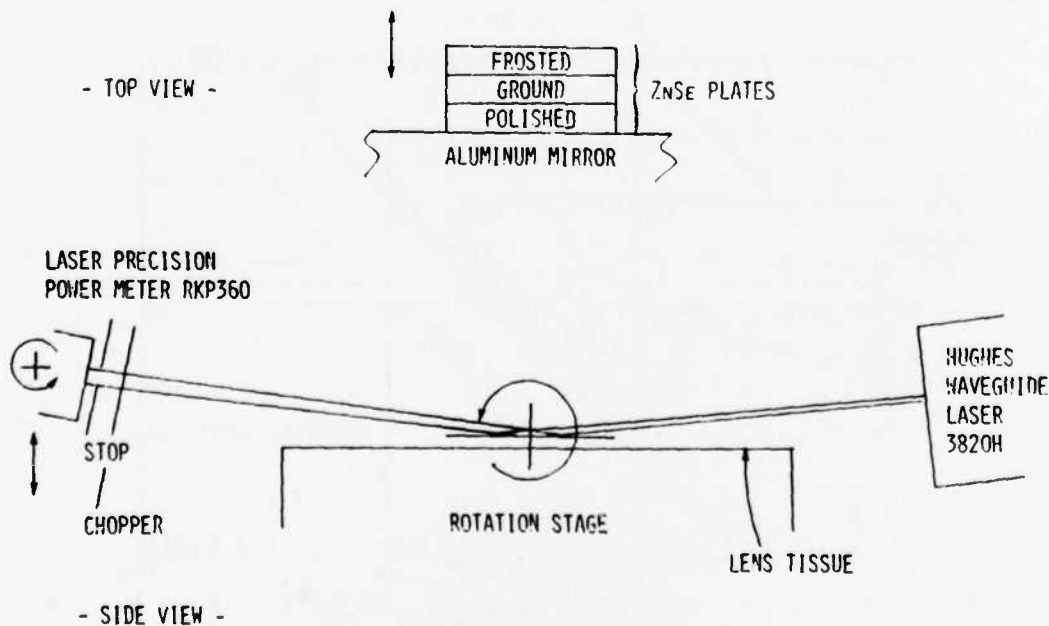
Figure 4.1.   Reflectivity Experimental Setup

-14-

The relative reflectivities as a function of angle of incidence are plotted in Fig. 4.2. A first surface S-polarization reflectivity curve and first surface P-polarization curve are also plotted with the data. The best fit origin for all five curves is at 102% indicating that the reference mirror reflectivity at near 90° incidence is actually 98% due to scratches and oxidation. It can be seen that with the ground surface finish the reflectivity has a loss of two percent or less as the incidence angle approaches 90°. Consequently, the easily machined ground surfaces were deemed satisfactory for use in the wave-guide laser experiments.

Figure 4.2. Experimental Results - ZnSe Reflection

In the case where a waveguide is bounded by an optically smooth, optically flat transparent plate of small wedge angle, multiple reflection interference effects must be taken into account when determining

-15-

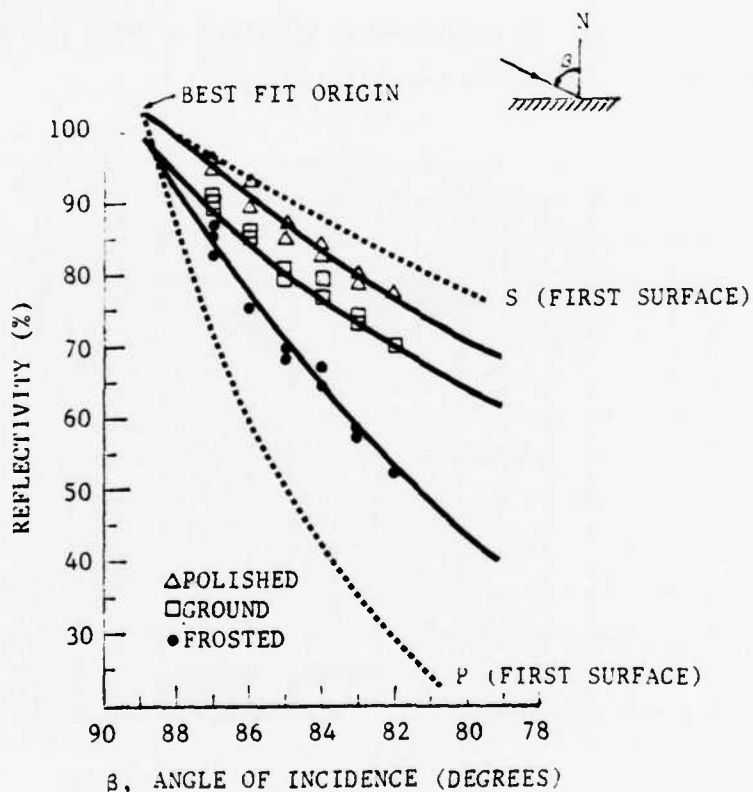the reflection coefficient. Dr. Glenn Zeiders performed an anlaysis on this problem and the results are shown in Fig. 4.3. The upper three curves are the S-polarization reflectivities, and the lower three curves are the P-polarization reflectivities. The highest curve in each set is the maximum of the coherent reflectivity curve, and the minimum is zero as indicated. This gives rise to the well known multiple reflection interference fringe effect. It is apparent that all six curves approach 100% reflectivity as the angle of incidence approaches 90°. Since the ZnSe plate material is not optical grade quality, we would expect reflectivities close to the first surface reflection curves. This is evidenced in the data of Fig. 4.2 where the first surface reflection curves are also plotted.
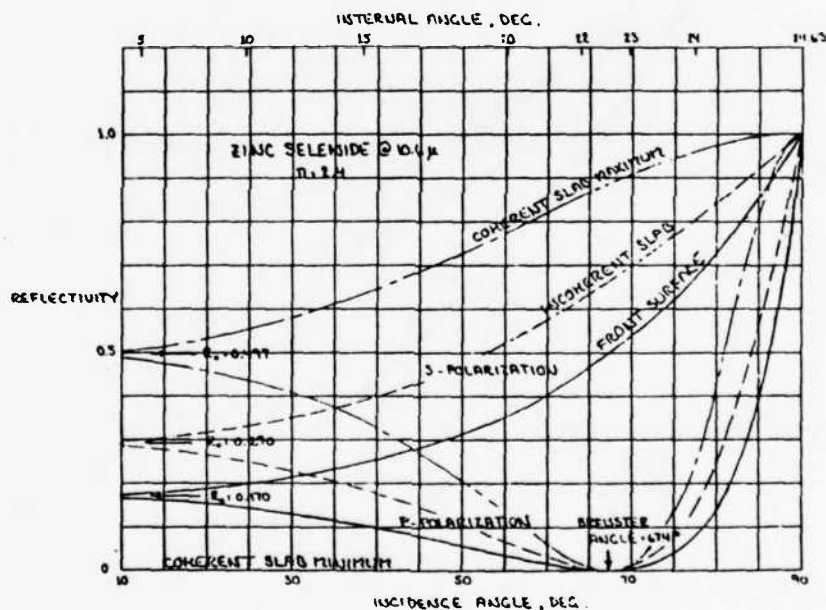
Figure 4.3. ZnSe Plate Reflectivity

In a related experiment a simple waveguide channel transmission test was made thorugh a 5cm long 1mm x 1mm ground channel in a ZnSe substrate. The experimental set up is shown in Fig. 4.4. The output of a commercial CO_2 laser is partially collected by the first waveguide

TOP VIEW

SIDE VIEW
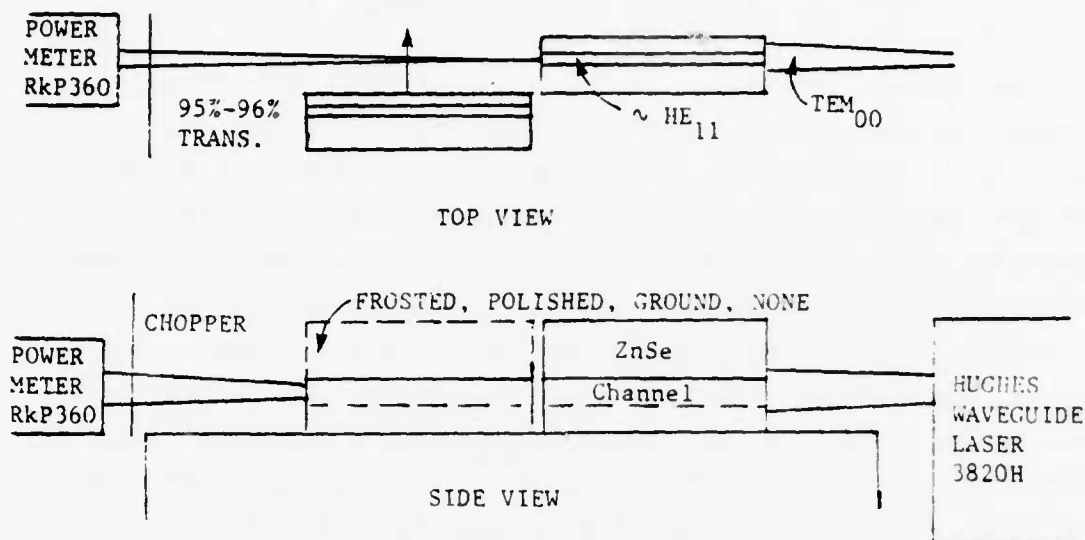
Figure 4.4. Simple Channel Transmission Test

channel. This forms a mode approximating an EH_{11} waveguide mode. A second channel is then inserted in series with the first. The transmission efficiency of the second waveguide was measured to be 95% to 96% of the incident pseudo EH_{11} mode. This simple test enforces the usability of inexpensive ground waveguide surfaces for the phase-locking experiment.

5.0 R.F. DISCHARGE EXCITATION EXPERIMENTS

The initial series of tests to demonstrate phase-locking of adjacent channel waveguide lasers followed the concept illustrated in Fig. 1.1. A number of ZnSe plates 50mm long, 11mm wide, and 2mm thick had five 1mm x 1mm grooves separated by 1mm ground on one side. One waveguide plate and a ZnSe cover plate were sandwiched between two electrodes. The waveguides and the RF electrodes are shown in Fig. 5.1. At each end of the waveguide channels were a ZnSe dielectric coated mirror. The waveguide array and electrode assembly were mounted on a mini-optical bench, and end mirrors supported by adjustable mirror mounts were also on the mini-optical bench. The entire assembly was placed in a 30cm long by 30cm diameter vacuum chamber shown in Fig. 5.2. The chamber was then readily filled with various He, N_2, CO_2 mixtures.

5 CHANNEL ZnSe CONFIGURATION

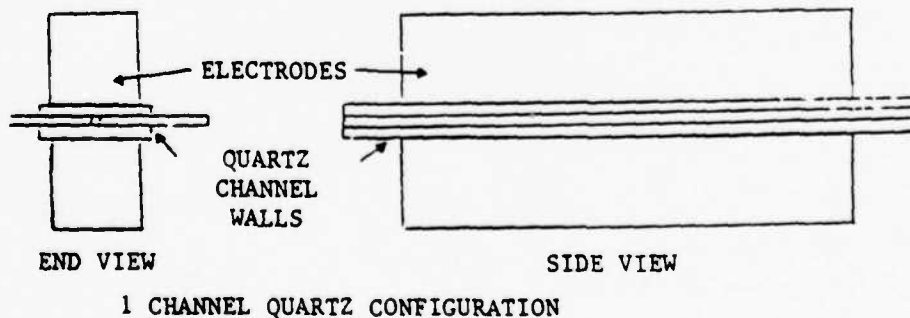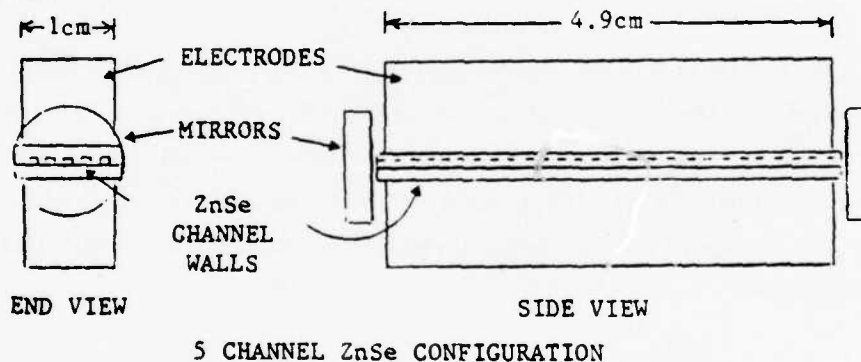1 CHANNEL QUARTZ CONFIGURATION

Figure 5.1. RF Excitation Waveguides
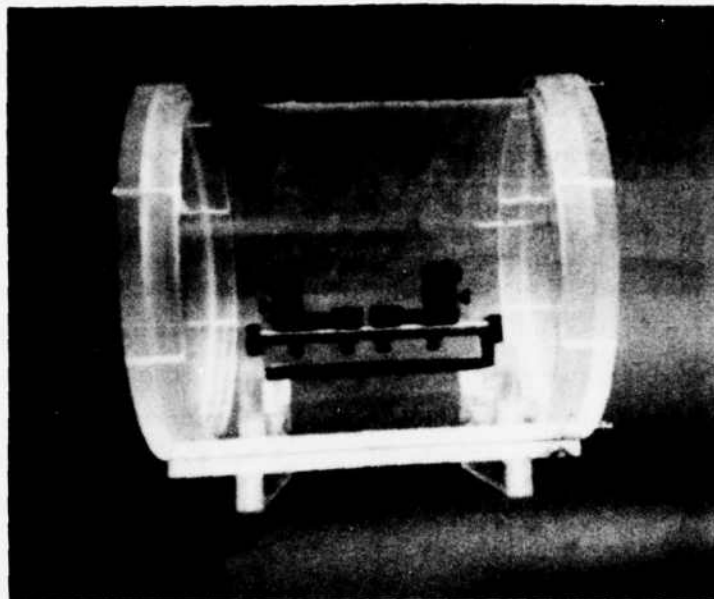
Figure 5.2.   Vacuum Chamber and Optical Bench

When RF power was applied to the electrodes, significant diffi-
culty was experienced in controlling the power loading inside the five
waveguides.   The RF discharge ignited around the sides and the ends of
the ZnSe plates preventing a transverse discharge inside the wave-
guides.   It had been expected that the longer path length around the
waveguide plates compared to the transverse distance through the wave-
guides and the lower impedance of the ZnSe compared to the laser gas
would minimize the discharge around the cavity.   Unfortunately, no RF
discharge inside any of the waveguides was achievable.

Next, a single waveguide formed of quartz glass slides was fabri-
cated as shown in the lower part of Fig. 5.1.   The quartz glass plates
extended an additional 1cm beyond the electrodes.   This prevented a
discharge around the sides of the waveguide plates, and a uniform
discharge in the cavity was observed.   When the cavity mirrors were
placed at each end of the waveguide, no lasing occurred at any gas
mixture or total pressure.   Laser power measurements were complicated

by the RF interference of the Laser Precision Radiometer (model RkP360/RL3610) that was to be used to detect lasing. Heat sensitive paper was used instead which would discolor at a laser output of about 0.1W. No such discoloration was observed.

It appeared that the cause of this inability to achieve lasing was due to excessive power loading of the gas inside the waveguide. Exact measurements of cavity input power loading were difficult to make. The reasons for the difficulty were associated with the much higher than expected standing wave ratio (SWR) in the electronic circuitry. The impedance matching transformer was expected to result in a SWR of 1.5 to 2, but values of 5 to 10 were measured, perhaps due to ignition of discharges around the waveuide cavity. For the single quartz waveguide the best estimate of power loading was about 15W, which was probably too much power to allow adequate heat removal through the quartz walls. The input power could not be regulated to lower power loadings without having the waveguide discharge extinguish.

These RF excitation difficulties thus led to a more conventional use of axial DC excitation with atmospheric pressure air as the insulating external gas to minimize ignition around the cavity. The design and successful results of this second phase device are discussed in the next section.

6.0 D.C. DISCHARGE EXCITATION DEVICE EXPERIMENTS

The use of a D.C. electric discharge down the length of a wave-
guide to excite the CO_2 gain medium is more staightforwardly imple-
mented and more controllable than the preceeding RF excitation tech-
nique. Since the purpose of this experiment is to prove the principle
of phase-locking of adjacent leaky waveguides, the more tractable exci-
tation method was tried next. Two devices were tested -- one 5cm long
and one 10cm long. The 10cm device was successfully phase-locked, and
the following sections pertain to the 10cm device except where indi-
cated.

6.1 Description of 5cm and 10cm Devices

A schematic diagram of the experimental two channel waveguide CO_2
laser is shown in Fig. 6.1. Two aluminum oxide plates 10cm long with
1mm square slots ground down the center form the waveguides. Three 1mm
diameter holes drilled into the waveguide from the outside are the gas
flow and electrical excitation ports. A ZnSe plate 10cm long and 1.4mm
thick polished on both sides is used as the "window" side of both wave-
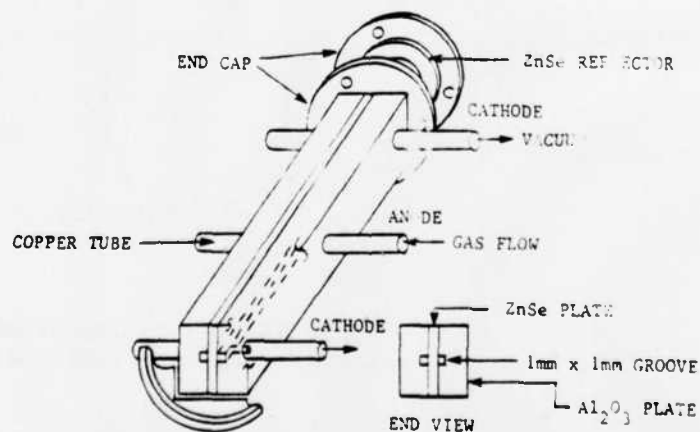guides. The ZnSe is not optical quality grade and no attempt to mini-

Figure 6.1. Cutaway Drawing of the Leaky Channel Waveguide CO_2 Laser

mize wedge-angle was made. The ZnSe plate is sandwiched between two Al_2O_3 plates as shown. Aluminum endcaps seal the lasers. Each endcap consists of a circular plate attached to the Al_2O_3 with a central rectangular hole and an o-ring groove surrounding it. An over size o-ring, a one inch diameter ZnSe reflecting element, and an annular retaining ring complete the endcap. Optical alignment is achieved by compressing the oversize o-rings. All joints are sealed with Epotek H77 high temperature epoxy.

Copper tubing is used both for the electrodes and the gas inlet and outlet ducts. The anodes are located in the centers of the wave-guides as shown in Fig. 6.2 and form the gas inlet ports. One cathode is located at each end of the waveguides and serves as the hot gas outlet port. A ballast resistance of 2MΩ for each half-waveguide dis-charge is sufficient for producing uniform discharges. Each waveguide has a separate power supply in order to permit individual control of the discharges.
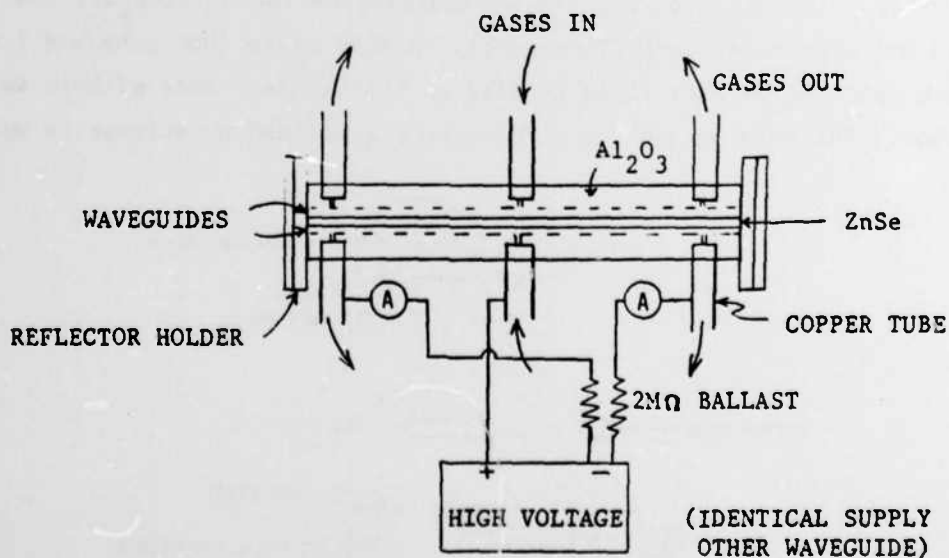

Figure 6.2. 10cm Waveguide Device and Power Supplies

-22-

6.2 Maximum Output Power Operating Conditions

Gas flow into the waveguides is controlled by separate needle valves. This allows easy power optimization by changing gas ratios as well as total pressure. The optimum gas ratio was found to be $3:1:1::He:N_2:CO_2$ at 150 torr inlet pressure for the 10cm device. This is very close to the published optimum values[2/12] for waveguide CO_2 lasers. The 150 torr inlet pressure corresponds to about a 100 torr pressure inside the waveguide based on the data of reference 13. Optimum discharge current is from 3.0 to 3.5mA per $(1mm)^2$ waveguide. Volumetric power loading at these currents corresponds to a $j \cdot E$ of 520 W/cc at an E/n of $4.5 \times 10^{-16}V$ cm^2.

In Fig. 6.3 is a plot of output power versus output coupling for hot waveguides that have been operated for about 15 minutes. An output coupling of 4% (ρ = 96%) is near optimum when using a maximum reflectivity (ρ = 99.2%) reflector at the other end. Under these conditions,
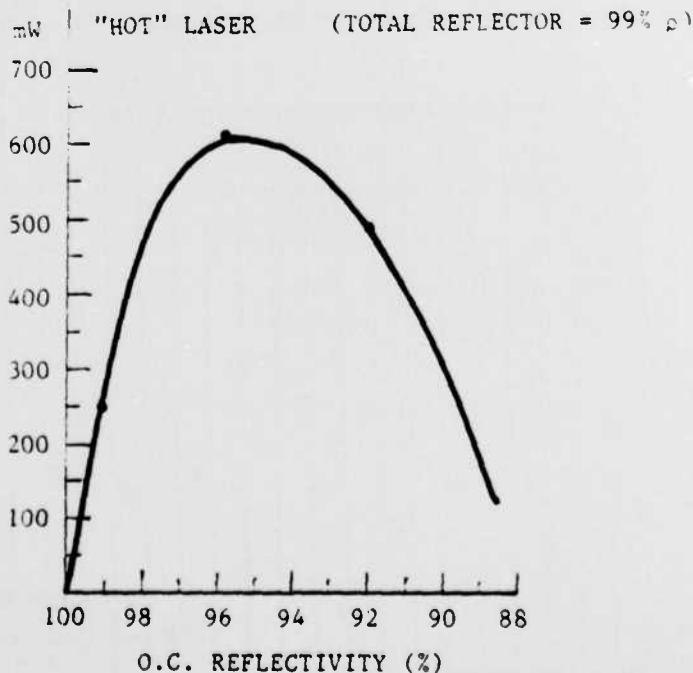

Figure 6.3. Power Output vs Output Coupling

-23-

950mW output power was measured on both the R(20) and the R(22) transitions (10.4μm band) with <u>cold</u> waveguides. The output power drops to about 50% of the initial output power after five minutes of operation due to wall heating of the gas since there is no external cooling system.

6.3 Lasing Transitions Observed

When two 99% reflectivity mirrors are place on both ends of the waveguides, many lasing transitions are observed as the cavity Fabry-Perot modes are thermally swept over the transition gain curves. As shown in Fig. 6.4, a total of 30 transitions were observed ranging from R14 to R26 and P14 to P30. Fortunately, at a more optimal output coupling of 4% (96% reflectivity), fewer transitions have enough gain to overcome the additional losses. In Fig. 6.5 a total of six transitions in one waveguide and eight transitions in the other are thermally scanned. The repetition of the gain curves corresponds to a free spectral range of the waveguide cavity of $C/2L = 1400$MHz. The lasing linewidth of the largest gain curve is thus measured to be 450MHz.
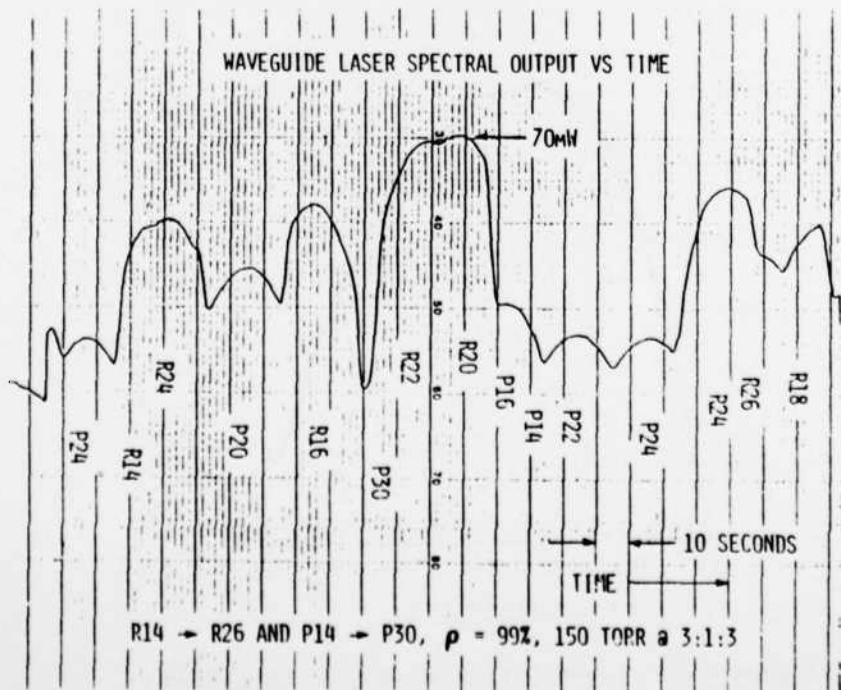

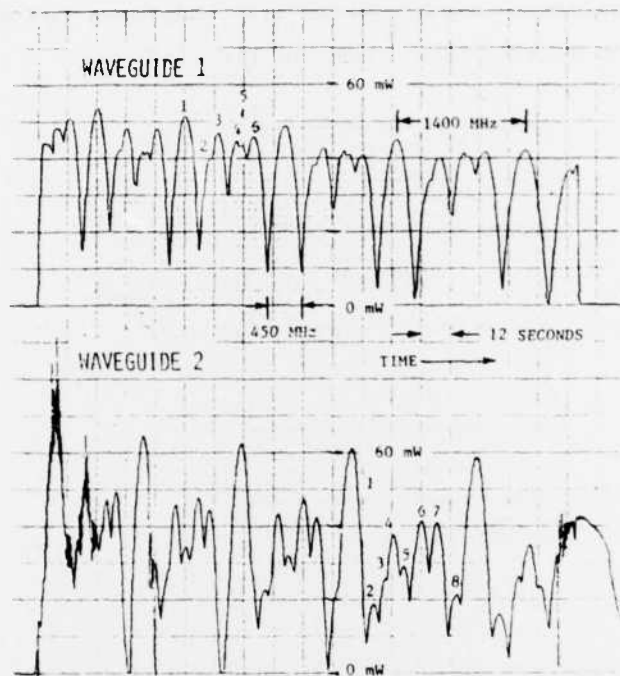Figure 6.4. Lasing Transitions

-24-

Figure 6.5. Simultaneous Waveguide Outputs

The spectral outputs of the two waveguide lasers were measured sequentially since both outputs could not be input to the Laser Engineering CO_2 Laser Spectrum Analyzer at the same time. Thus, it was not possible to determine if the same transitions were lasing simultaneously. Looking at the independent and uniform output power curves of Fig. 6.5, however, it becomes apparent that the two lasers have no chance of phase-locking unless both lasers are operating on the same transition.

6.4 Output Polarization

The polarization of the leaky-waveguide lasers was found to be parallel to the ZnSe plate surface in the x direction with a polarization ratio of at least 200:1::x:y. Since the S polarization (see section 4.0) has higher reflectivity than the P polarization at large angles of incidence (~ 90°) with the normal to the ZnSe plate, the S

-25-

polarization radiation has the lower loss and forms the dominant mode. The polarization direction is shown in Fig. 6.6.
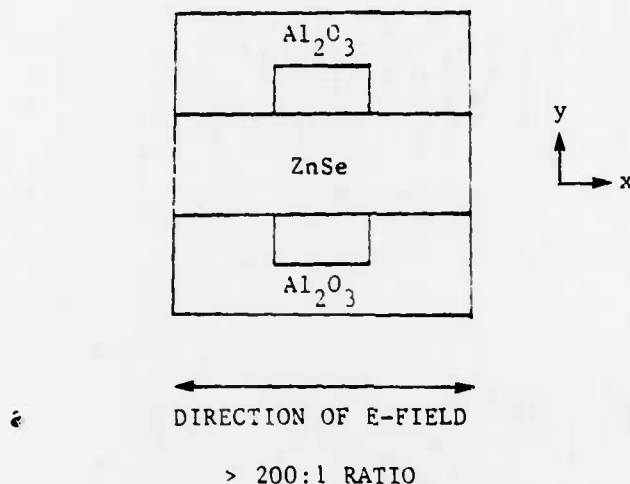

Figure 6.6. Polarization of Laser Output

6.5 Heterodyne Experiments

The outputs of the two lasers were propagated a distance of one meter to a liquid nitrogen cooled HgCdTe photodiode detector. At this distance the modes are about 4cm in diamter, and there is considerable overlap since the optical axes are only 2.4mm apart. Also, at this distance the waveguides are nearly planar (eq. (17)), and any bea frequency would be readily observable. In fact, however, after several hours of observation no beat frequencies were observed. This indicates that a) each waveguide is operating single mode with no intermode beating and b) that if both lasers were operating on the same transition they were phase-locked so no beat frequency would be present. (Note that operation on two different CO_2 transitions would result in at least a 40,000MHz, random phase beat frequency -- far too fast for the 200MHz detector.) More conclusive evidence of phase-locking is given in the next section.

6.6 Output Spatial Distribtion - Phase-Locking

The spatial distribution of the outputs of the two waveguide
lasers was measured using a Spiricon 64 element scanning pyroelectric
array. Each element is 85μm x 100μm on 100μm centers. As the two
lasers thermally drift over 6 to 8 lasing transitions each, the EH_{11}
waveguide modes propagate outward and typically produce a noncoherent
summation shown in Fig. 6.7A. The two modes are partially focussed in
this figure for clarity. Interference fringes between lasers on
different transitions would be changing at a rate equal to the fre-
quency difference of the lasing transitions, at least 40,000MHz, far
too fast for detection by the detector array. The upper trace of Fig.
6.7A corresponds to the heating of the pyroelectric elements and the
lower trace to their cooling.

When the two lasers are operating on the same transition, station-
ary interference fringes are observed as shown in Fig. 6.7B at a dis-
tance of $z = 35cm$ (unfocussed). These fringes remain unchanged for a
period of a minute until one laser jumps to another transition. Vary-
ing the discharge current in one waveguide rapidly from 1mA to 7mA did
not affect the fringe pattern, producing only a small amplitude change.
Ordinarily a frequency change of about 1.5MHz/mA[14] or a 9MHz heterodyne
signal (rapid fringe movement) would have been observed. Since no
relative phase change (fringe shift) or beat frequency (fringe veloc-
ity) is observed, we conclude that the two waveguide lasers are phase-
locked.

We repeat Fig. 6.7A and B in Fig. 6.8 with the laser modes
unfocussed. Fig. 6.7A is the intensity distribution of the unfocussed
left laser waveguide and 6.7B is that of the unfocussed right wave-
guide. Unfortunately, multiple reflections between the front surface
of the $LiTaO_3$ detector and the near surface of the Ge window causes
small interference effects on the nearly planar waves. The important
features are clearly visible, however. In Fig. 6.8C is repeated a
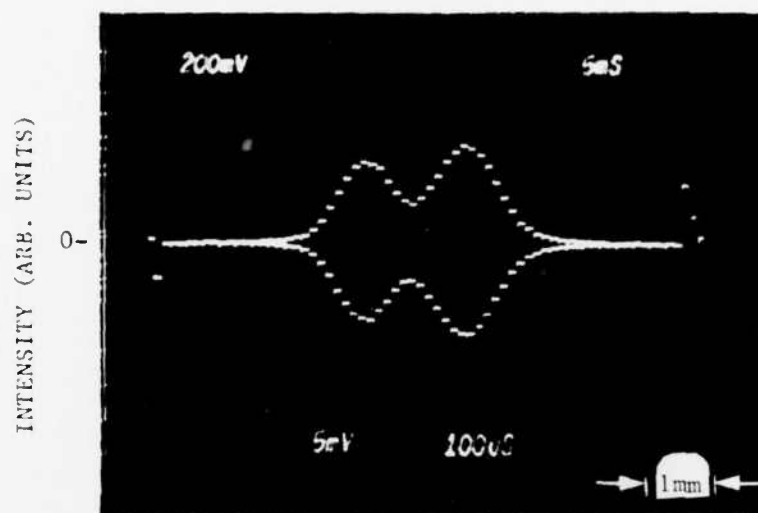
Figure 6.7A. Typical noncoherent summation, partially focussed for clarity. Horizontal scale corresponds to horizontal direction in Fig. 1.1.
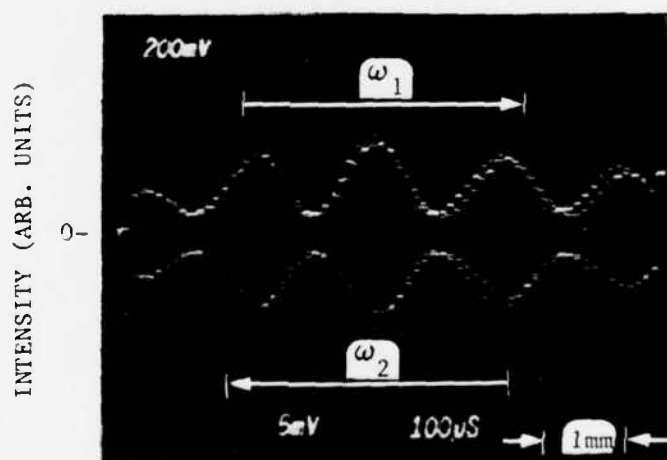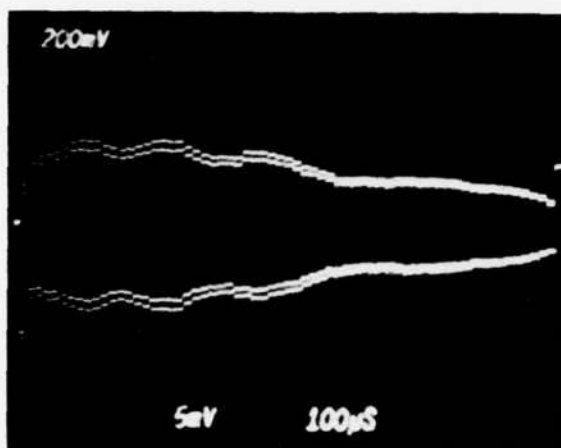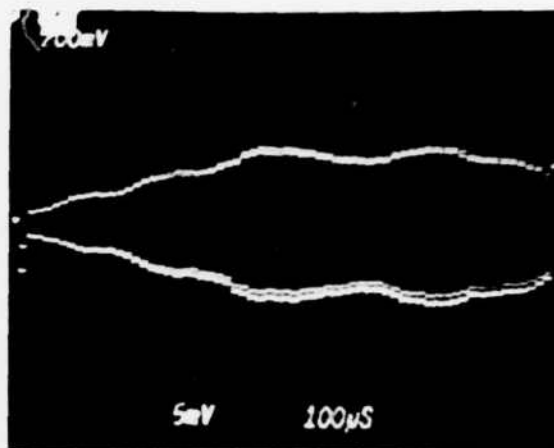

Figure 6.7B. Coherent summation of two waveguide lasers unfocussed at 35cm from the output aperture. Horizontal scale corresponds to horizontal direction in Fig. 1.1.
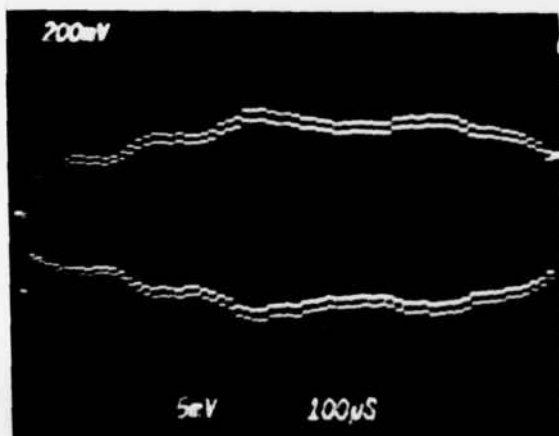
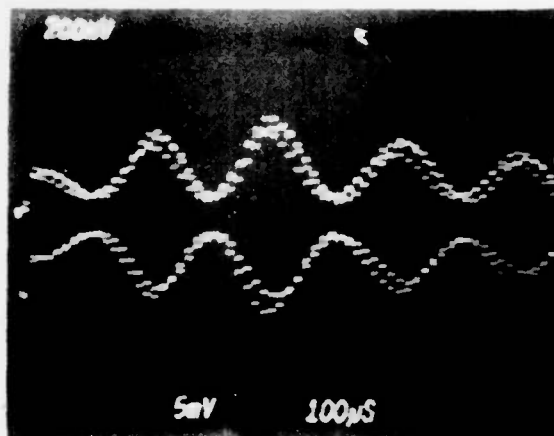Figure 6.7. Nohcoherent and Coherent Summation of Laser Outputs

A. LEFT WAVEGUIDE

B. RIGHT WAVEGUIDE

C. TYPICAL NONCOHERENT SUMMATION

D. COHERENT SUMMATION

Figure 6.8. Waveguide Laser Interference Patterns

typical noncoherent summation, unfocussed. In 6.8D the coherent inter-
ference pattern is repeated for reference. The effect is unmistakeable
in the unfocussed intensity distribuitons.

The shape of the expected interference pattern can be straight-
forwardly calculated. Laakman and Steier[5] and Henderson[6] have shown
that a TEM_{00} spot size of $\omega_0 = 0.70a$ is the best approximation to the
EH_{11} mode of a square hollow waveguide of half-width a. From Gaussian
mode theory[15] the electric field from the ith waveguide may be written
(assuming no phase or frequency differences) suppressing the exp $j\omega t$
terms

$$\vec{E}_i = \left(A_i \hat{x} + B_i \hat{y} \right) \frac{\omega o}{\omega(z)} \exp\left(- \frac{x^2 + y_i^2}{\omega(z)^2} \right) \exp\left(-jkz + j \tan^{-1}\left(\frac{z}{z_R} \right) \right) \tag{15}$$

$$x \exp\left(-j \frac{k(x^2 + y_i^2)}{2R(z)} \right)$$

where

$$\omega^2(z) = \omega_o^2 + (\lambda/\pi\omega_o)^2 z^2 \quad \text{mode radius} \tag{16}$$

$$R(z) = z + z_R^2/z \quad \text{phase front curvature} \tag{17}$$

$$z_R = \pi\omega_o^2/\lambda = 3.5cm \quad \text{Rayleigh range} \tag{18}$$

Here y is in the horizontal direction of Figs. 1.1, 6.7 and 6.8, and
taking a coordinate system at the center of the array, $y_1 = y + \rho/2$ and
$y_2 = y - \rho/2$ where ρ is the waveguide center to center distance of
2.4mm. Summing the x polarization components and multiplying by the
complex conjugate, the interference term of the intensity distribution
assuming equal amplitudes is

$$\left|\left(\vec{E}_1 + \vec{E}_2\right)_{\hat{x}}\right|^2 \propto 2 \exp\left(-2y^2/\omega(z)^2\right)\left(1 + 2y^2\rho^2/\omega(z)^4 + \cos\left(\frac{k\rho y}{R(z)}\right)\right) \quad (19)$$

for $y \ll \omega^2(z)/\sqrt{2}\,\rho$. There is a central $(y = 0)$ maximum when both lasers are in phase which is evidenced in Fig. 6.7B. The maximum is four times that of a single laser. Fringe separation is

$$2y(\min) = \frac{\lambda R(z)}{\rho} = 1.56\text{mm} \quad (20)$$

From Fig. 6.7B the fringe separation at $z = 35$cm is seen to be 16 elements or 1.6mm, also verifying phase-locking.

6.7 Cavity Coupling Measurement

Power coupling from the lasing waveguide into the nonexcited, cold waveguide was measured by centering a razor blade slit 1mm wide 1cm from the output aperture of the cold waveguide as shown in Fig. 6.9. A radiometer was located an additional 10cm from the slit. The power coupled into a cold waveguide mode was measured to be about 4×10^{-4} of the power in the lasing waveguide. The polarization of the coupled radiation was not measured.
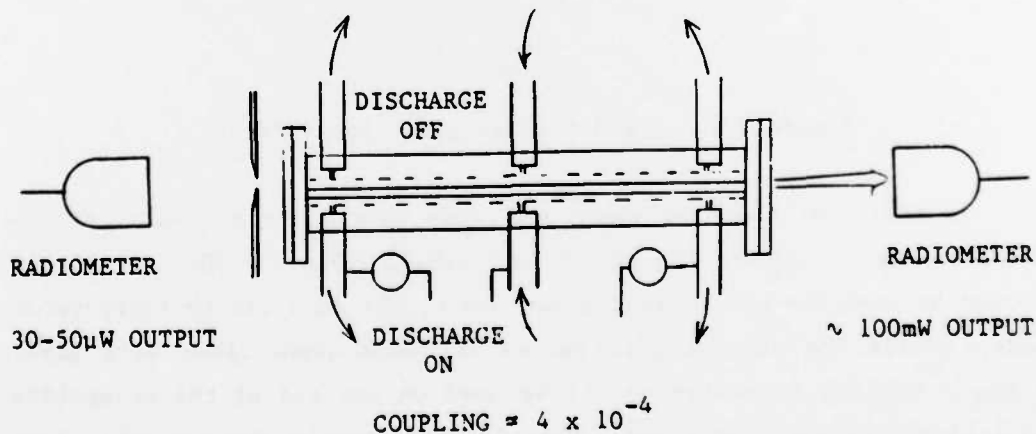

Figure 6.9. Waveguide Coupling Experiment

-31-

7.0 FUTURE WORK

The next step in building an n x m array of phase-locked waveguide lasers is to demonstrate phase-locking in two directions. A two by three waveguide array is recommended as shown in Fig. 7.1. D.C. excitation would again be used, and water cooling of the outer surfaces of the waveguide structure would be provided. Materials less expensive than ZnSe such as KCl and BaF_2 should be investigated.
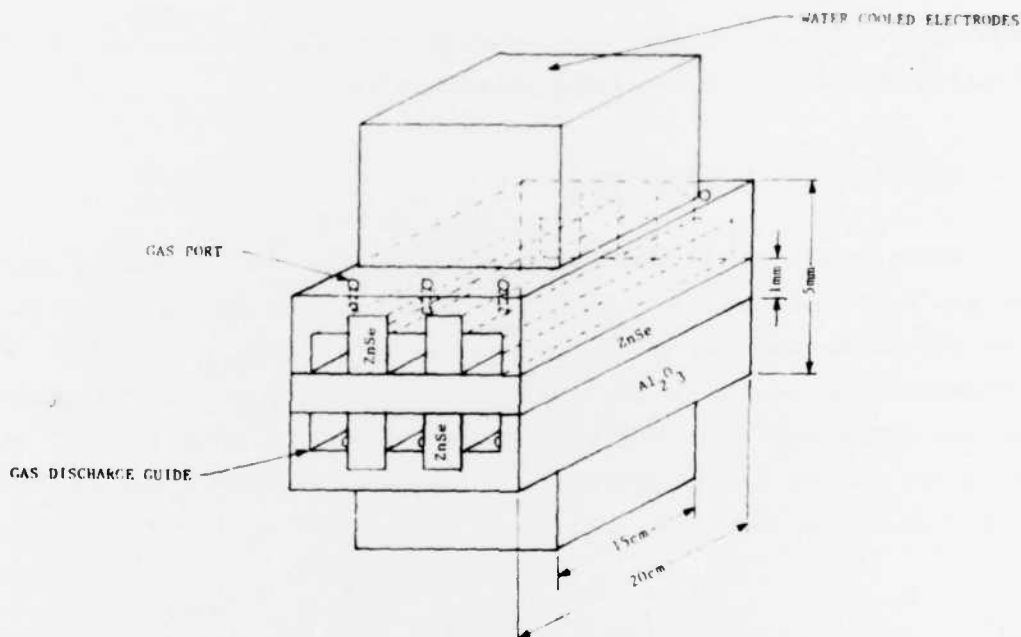
Figure 7.1. 2 x 3 CO_2 Waveguide Laser Array

In addition, the next waveguide array should force common transition lasing. Longer waveguides of perhaps 20cm to 30cm in length should be used for more output power and to put more cavity Fabry-Perot modes inside the various gain curves so fewer transitions will lase. Also, a grating or etalon should be used on one end of the waveguides to select a single transition. This is conceptually shown in Fig. 7.2. Also shown is a PZT translator for controlling the cavities' lengths in order to compensate for thermal expansion. Such a test device should

-32-

Figure 7.2. Conceptual Waveguide Laser Array Optical Bench

preceed or be tested in conjuction with RF excitation of large arrays
of waveguide lasers.

REFERENCES

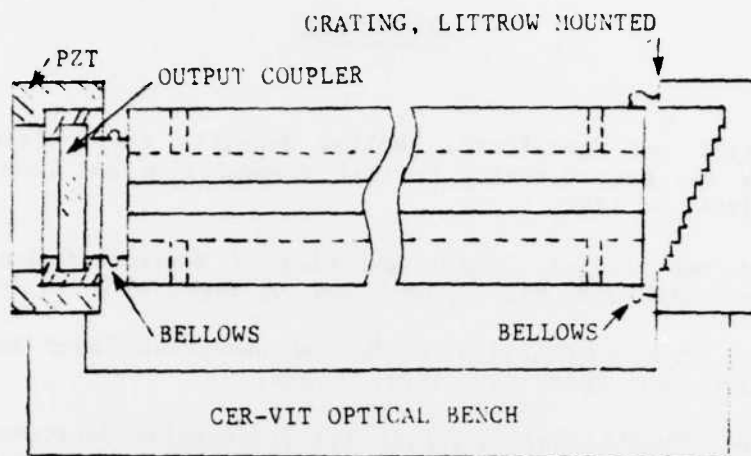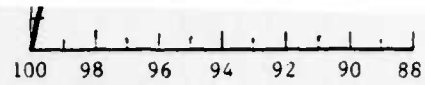1. Marcatili and Schmeltzer, "Hollow Metallic and Dielectric Wave-guides for Long Distance Optical Transmission and Lasers," BSTJ, July 1964, p. 1783.

2. Abrams and Bridges, "Characteristics of Sealed-Off Waveguide CO_2 Lasers," IEEE JQE, Vol. 1, OE-9, No. 9, Sept. 1973, p. 940.

3. Abrams, "Coupling Losses in Hollow Waveguide Laser Resonators," IEEE JQE, Vol. QE-8, Nov. 1972, p. 838.

4. Krammer, "Field Configurations and Propagation Constants of Modes in Hollow Rectangular Dielectric Waveguides," IEEE JQE, Aug. 1976, p. 505.

5. Laakman and Steier, "Waveguides: Characteristic Modes of Hollow Rectangular Dielectric Waveguides," Applied Optics, Vol. 15, No. 5, May 1976, p. 1334.

6. Henderson, "Waveguide Lasers with Intracavity Electro-Optic Modula-tors: Misalignment Loss," Applied Optics, Vol. 15, No. 4, April 1976, p. 1066.

7. Degnan and Hall, "Finite Aperture Waveguide Laser Resonator," IEEE JQE Vol. QE-9, No. 9, Sept. 1973, p. 901.

8. Rigrod, "Saturation Effects in High Gain Lasers," Journal of Applied Physics, Vol. 36, Aug. 1965, p. 2487.

9. Casperson, "Laser Power Calculations: Soures of Error, " Applied Optics, Vol. 19, No. 3, 1 Feb. 1980, p. 422.

10. Cohen, "Waveguide CO_2 Laser Gain: Dependence on Gas Kinetic and Discharge Properties," IEEE JQE, Vol. QE-12, No. 4, April 1973, p. 237.

11. Douglas-Hamilton, Lawder, "CO_2 Electric Discharge Laser Kinetics Handbook," AFWL-TR-74-216, April 1975.

12. Stein, "Gain-Optimized CO_2 Waveguide Laser," IEEE JQE 18, 1982, p. 1321.

13. Smith, Maloney, and Wood, Appl. Phys. Lett. 23, 1973, p. 524.

14. Product Bulletin, Apollo Lasers, Inc., 1982.

15. Siegman, Introduction to Laser and Masers, McGraw-Hill, New York, 1971, p. 304.

Figure 6.2.   10cm Waveguide Device and Power Supplies

Figure 6.2.   10cm Waveguide Device and Power Supplies

$$100 \quad 98 \quad 96 \quad 94 \quad 92 \quad 90 \quad 88$$

O.C. REFLECTIVITY (%)

Figure 6.3. Power Output vs Output Coupling

-23-

100   98   96   94   92   90   88

O.C. REFLECTIVITY (%)

Figure 6.3. Power Output vs Output Coupling

R14 → R26 AND P14 → P30, ρ = 99%, 150 TORR a 3:1:3

10 SECONDS

TIME

Figure 6.4. Lasing Transitions

tion ratio of at least 200:1::x:y. Since the S polarization (see
section 4.0) has higher reflectivity than the P polarization at large
angles of incidence (~ 90°) with the normal to the ZnSe plate, the S

the 200MHz detector.)   More conclusive evidence of phase locking

given in the next section.

the 200MHz detector.)   More conclusive evidence of phase locking

given in the next section.

of the $LiTaO_3$ detector and the near surface of the ...
small interference effects on the nearly planar waves. The important
features are clearly visible, however. In Fig. 6.8C is repeated a

of the $LiTaO_3$ detector and the near surface of the ...
small interference effects on the nearly planar waves. The important
features are clearly visible, however. In Fig. 6.8C is repeated a